



Seasonal and interannual variations of top-of-atmosphere irradiance and cloud cover over polar regions derived from the CERES data set

Seiji Kato,¹ Norman G. Loeb,² Patrick Minnis,² Jennifer A. Francis,³ Thomas P. Charlock,² David A. Rutan,⁴ Eugene E. Clothiaux,⁵ and Szedung Sun-Mack⁶

Received 24 April 2006; revised 21 July 2006; accepted 21 August 2006; published 4 October 2006.

[1] The daytime cloud fraction derived by the Clouds and the Earth's Radiant Energy System (CERES) cloud algorithm using Moderate Resolution Imaging Spectroradiometer (MODIS) radiances over the Arctic from March 2000 through February 2004 increases at a rate of 0.047 per decade. The trend is significant at an 80% confidence level. The corresponding top-of-atmosphere (TOA) shortwave irradiances derived from CERES radiance measurements show less significant trend during this period. These results suggest that the influence of reduced Arctic sea ice cover on TOA reflected shortwave radiation is reduced by the presence of clouds and possibly compensated by the increase in cloud cover. The cloud fraction and TOA reflected shortwave irradiance over the Antarctic show no significant trend during the same period.

Citation: Kato, S., N. G. Loeb, P. Minnis, J. A. Francis, T. P. Charlock, D. A. Rutan, E. E. Clothiaux, and S. Sun-Mack (2006), Seasonal and interannual variations of top-of-atmosphere irradiance and cloud cover over polar regions derived from the CERES data set, *Geophys. Res. Lett.*, 33, L19804, doi:10.1029/2006GL026685.

1. Introduction

[2] Passive microwave measurements from satellites indicate that the Arctic perennial sea ice extent decreased at a rate of 6.4% per decade from 1978 through 2000 [Comiso, 2002]. A more recent analysis by Stroeve *et al.* [2005] reveals that the September ice extent is decreasing even faster, at a rate of 7.7% per decade. Rothrock *et al.* [1999] show that the mean draft of Arctic sea ice has decreased by about 40% between 1958–1976 and 1990s. All these studies indicate that Arctic sea ice cover is decreasing rapidly. Because a changing sea ice cover affects surface albedo, understanding the impact of this change on the top-of-atmosphere (TOA) shortwave and longwave irradiances and other related atmospheric properties is important for assessing changes in the Arctic radiation budget. The

Clouds and the Earth's Radiant Energy System (CERES) instruments [Wielicki *et al.*, 1996] and Moderate Resolution Imaging Spectroradiometer (MODIS) [King *et al.*, 1992] on NASA's *Terra* platform have obtained measurements since March 2000 and those on the *Aqua* platform have obtained measurements since August 2002. These instruments provide an opportunity to investigate the changes in TOA irradiance and atmospheric property associated with the recent period of rapid change in snow and sea ice cover.

[3] Identifying clouds over bright snow and sea ice surfaces and estimating irradiances from radiance measurements over polar regions are challenging obstacles to monitoring changes in TOA irradiance and atmospheric properties. Cloud identification over sea ice, however, is expected to have improved with the increased number of spectral channels on MODIS and the capability to detect cloud trends has been enhanced by reliable calibrations of all MODIS and CERES channels [Loeb *et al.*, 2006a]. Hollinger *et al.* [1990] have also shown that the Special Sensor Microwave/Imager (SSM/I) is a stable microwave system.

[4] The error in estimating TOA irradiances from radiances measured by the CERES instruments is smaller than the error in Earth Radiation Budget Experiment (ERBE) irradiance estimates [Loeb *et al.*, 2006b]. This is largely due to two factors: better scene identification and better angular distribution models. The scene within an approximately 20 km CERES footprint is identified at a smaller scale (≈ 1 km) using collocated MODIS-derived cloud and aerosol properties. SSM/I-derived snow and sea ice fractions are also collocated within the CERES footprints, which helps in identifying seasonal snow and sea ice cover. Improvements in the irradiance estimates from ERBE to CERES are significant over polar regions [Loeb *et al.*, 2006b], as ERBE had known problems in distinguishing clouds from snow and sea ice. In this study, we investigate the TOA radiation budget difference between the Arctic and Antarctic. We also investigate how TOA shortwave irradiance and cloud cover vary with the sea-ice cover changes that have occurred over ocean and land in these regions since 2000.

2. Methods

[5] We use data collected by MODIS and the CERES cross-track instruments on NASA's *Terra* satellite from March 2000 through February 2004 and on *Aqua* from August 2002 through February 2004. Both *Terra* and *Aqua* data are used to determine seasonal variations in cloud properties and TOA irradiances, but only *Terra* data are used for the trend analysis. The cloud properties, specifically cloud fraction, in this study are derived from MODIS

¹Center for Atmospheric Sciences, Hampton University, Hampton, Virginia, USA.

²Climate Science Branch, NASA Langley Research Center, Hampton, Virginia, USA.

³Institute of Marine and Coastal Sciences, Rutgers University, New Brunswick, New Jersey, USA.

⁴Analytical Services and Materials, Inc., Hampton, Virginia, USA.

⁵Department of Meteorology, Pennsylvania State University, University Park, Pennsylvania, USA.

⁶Science Applications International Corporation, Hampton, Virginia, USA.

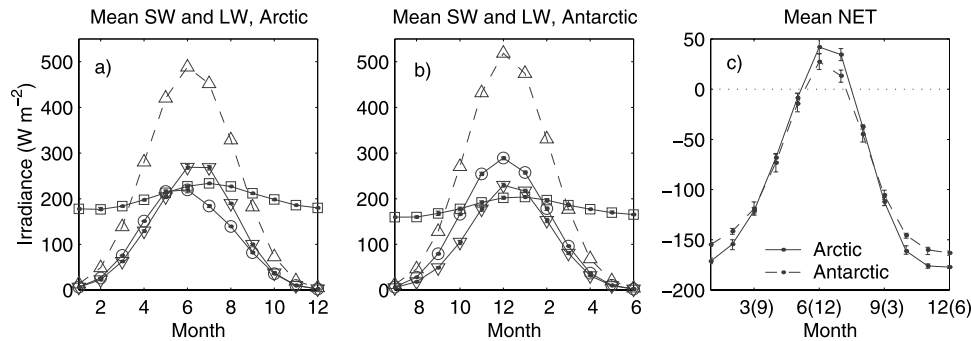


Figure 1. Monthly mean TOA reflected shortwave irradiances (open circles), absorbed shortwave irradiance (open downward triangles), longwave irradiances (open squares) and downward shortwave irradiances (open upward triangles) for (a) the Arctic (between 60°N and 90°N), for (b) the Antarctic (between 60°S and 90°S), and (c) Net irradiance (absorbed shortwave irradiance - longwave irradiance) at the top of the atmosphere; the months in parentheses are for the Antarctic. The vertical bars represent the maximum and minimum values for a given month as derived from Terra and Aqua CERES data.

irradiance using the algorithms described by *Minnis et al.* [2003]. Hereafter, these products are denoted as cloud products derived from the CERES cloud algorithm. The TOA shortwave and longwave irradiances are derived from CERES radiance measurements using angular distribution models described by *Loeb et al.* [2005] and *Kato and Loeb* [2005]. All irradiances and cloud properties are taken from the Single Scanner Footprint (SSF) Eddition2B_{Rev1} product for *Terra* and Eddition1B product for *Aqua*, which are available from the NASA Langley Atmospheric Science Data Center.

[6] The daily mean TOA shortwave irradiance is estimated from the instantaneous shortwave irradiance assuming that atmospheric, cloud, and surface properties are constant throughout a 24-hour period. For a given instantaneous irradiance, the corresponding daily mean irradiance is given by integrating the irradiance over all daylight hours using the solar-zenith-angle dependent albedo from angular distribution models for snow and sea ice from *Kato and Loeb* [2005] and for land and ocean from *Loeb et al.* [2003]. Therefore, all instantaneous irradiances have corresponding daily mean values. No correction is made to the longwave irradiance to account for diurnal variations. Changes in either shortwave or longwave irradiances over the course of each day due to variations in the atmospheric and surface properties are implicitly taken into account because measurements are taken at many different times of day in polar regions by both *Terra* and *Aqua*.

[7] All daily mean irradiances derived from CERES data are averaged over 1° × 1° grid boxes and then averaged over a month. To obtain a mean irradiance for 60°N to 90°N, hereafter the Arctic, and 60°S to 90°S, hereafter the Antarctic, 1° × 1° regional values are area weighted and averaged. To determine the mean cloud fraction over a 1° × 1° grid box, the number of MODIS cloudy pixels is divided by the total number of MODIS pixels in the box. The cloud fraction over the Arctic and Antarctic is then the area-weighted average of cloud fractions over all relevant 1° × 1° grid boxes. Sea ice and snow fractions are derived from SSM/I data, which are included in the SSF data set. Similar to the cloud fraction, SSM/I-derived snow and sea ice fractions over a CERES footprint are converted into an

equivalent number of 1-km pixels with snow and sea ice by multiplying the snow and ice fraction by the total number of 1-km pixels over the CERES footprint. The snow and sea ice fractions over a 1° × 1° grid box are then derived by dividing the number of snow and sea ice 1-km pixels by the total number of 1-km pixels in the box. Note that the SSM/I-derived snow and sea ice fractions are not available within 50 km of the coastline. The snow and sea ice fractions in the coastal region are, therefore, not included in this analysis.

[8] The monthly mean TOA shortwave and longwave irradiances and cloud amounts for the four-year period are derived by averaging the four values from the four years. Anomalies are determined by subtracting the four-year monthly mean value from the monthly value for each year.

3. Seasonal Variations

[9] The monthly mean reflected and absorbed shortwave irradiances and longwave irradiances show similar seasonal variations for both the Arctic and Antarctic (Figure 1). The month with the maximum reflected shortwave irradiance coincides with the month with the maximum TOA downward irradiance for both the Arctic (June) and Antarctic (December). This agrees with *Curry and Ebert* [1992], who show that the maximum reflected shortwave irradiance at 80°N latitude occurs in June. It also agrees with the results of *Wang and Key* [2005a], who estimated the shortwave irradiances from the Advanced Very High Resolution Radiometer (AVHRR). The maximum (minimum) absorbed shortwave irradiance occurs in June (December) for the Arctic and December (June) for the Antarctic. The absorbed shortwave irradiance in July over the Arctic is nearly equal to that in June because the July surface albedo is lower due to melting sea ice. The longwave irradiance maximum (minimum) over the Arctic occurs in July (February) and over the Antarctic in January (July), approximately one month after the corresponding maxima (minima) in the absorbed shortwave irradiance. Net irradiance is positive for two months in the summer over both polar regions.

[10] While the seasonal cycles for the Arctic and Antarctic are similar, the values are different. The annual average CERES-derived TOA downward shortwave irradiances,

Table 1. Annual Mean TOA Irradiances and Albedos^a

TOA Irradiances and Albedo	Arctic (60°N–90°N)	Antarctic (60°S and 90°S)
Downward shortwave (Wm^{-2})	204.2 (201.3)	206.8 (202.5)
Shortwave albedo	0.469 (0.487)	0.566 (0.591)
Upward longwave (Wm^{-2})	201.1 (201.2)	179.8 (179.8)
Net (Wm^{-2})	-92.6 (-97.9)	-90.1 (-97.0)

^aNumbers in parentheses are from ERBE angular distribution models applied to CERES data. The differences in the CERES and ERBE TOA downward shortwave irradiances are due to using spatially and temporally coarse ERBE values in the average.

shortwave albedos, TOA upward longwave irradiances, and TOA net irradiances are shown in Table 1, along with the values estimated from the ERBE-like product ES4 that uses ERBE angular distribution models applied to CERES radiances. Compared to the Antarctic, a larger positive net irradiance during Arctic summer is offset by a larger negative net irradiance during Arctic winter (Figure 1c). As a result, the annual average net irradiances for the two regions are nearly equal, -92.6 Wm^{-2} for the Arctic and -90.1 Wm^{-2} for the Antarctic. This result indicates that the annual average energy transports to the Arctic and Antarctic are nearly equal and that about 50% of the energy emitted by the polar regions is supplied by dynamical processes that transport energy from mid-latitude regions.

[11] The CERES cloud fraction retrieved from MODIS shows an increase from approximately 0.5 in winter to about 0.8 in summer over the Arctic (Figure 2a). The cloud fraction maximum occurs in September when the snow and sea ice fractions are lowest. The seasonal variation of the Arctic cloud fraction is qualitatively in agreement with the cloud fraction derived from AVHRR polar pathfinder data [Wang and Key, 2005a] and surface observations [Hahn et al., 1995]. The cloud fraction derived by International Satellite Cloud Climatology Project (ISCCP) [Schiffer and Rossow, 1983] over the Arctic for the same four-year period shows no seasonal cycle and that derived from TOVS [Schweiger et al., 2002] has more clouds in winter than in summer. The summertime cloud fraction derived by ISCCP and from TOVS are 0.06 lower than the cloud fraction derived by the CERES cloud algorithm. The ISCCP-derived and TOVS-derived cloud fractions are, however, approximately 0.2 and 0.3, respectively,

greater than the cloud fraction from the CERES cloud algorithm in winter. This difference could be due to TOVS' large footprint size (100 km) or greater sensitivity to thin clouds. All satellite cloud detections are subject to difficulties in discriminating between clear and cloudy conditions in the nocturnal Arctic atmosphere, which is often characterized by near-surface temperature inversions. The Arctic winter cloud fractions derived from both the CERES cloud algorithm and the MODIS Science Team Collection 4 algorithm [King et al., 2003] applied to Terra data, as well as an updated CERES algorithm that uses slightly different detection threshold values and channels applied to Aqua data, are approximately 0.4 to 0.6 and the minimum values occur in January. This contrasts with the AVHRR-derived cloud fraction of Wang and Key [2005a], which show a minimum during April.

[12] The seasonal variation of cloud fraction over the Antarctic (Figure 2b) is less pronounced than that over the Arctic. The mean cloud cover over Antarctic is relatively constant, ranging between 0.62 and 0.75 during all seasons. The weaker Antarctic seasonal variation results from somewhat opposite changes over land and ocean. The cloud cover over ocean varies from about 0.7 in winter to about 0.9 in summer, while for land it varies from 0.65 in winter to 0.45 in summer. The ocean-land cloud fraction contrast in the Antarctic is greater than the contrast in the Arctic, which is not surprising given that in the Arctic, both sea ice in ocean and snow over land melt in summer whereas in the Antarctic, only sea ice in ocean melts in summer.

[13] Beesley and Moritz [1999] suggest that the seasonal cycle of low-level Arctic cloud amount is largely due to microphysical processes. Low temperatures during winter allow ice crystals to grow larger, resulting in larger fall velocities and a reduction in cloud amount. From data taken during the Surface Heat Budget of the Arctic Ocean (SHEBA) project, Lin et al. [2003] found that relative humidity increases with surface temperature, especially when temperatures exceed 275 K. This implies that the frozen sea surface impedes the formation of low-level clouds. Further evidence of this effect is the peak cloud fraction from the CERES cloud algorithm occurring over both polar regions coincident with minimum sea ice coverage (Figures 2a and 2b). However, sea ice variability provides only a partial explanation for the land-ocean cloud fraction differences. Other factors that are

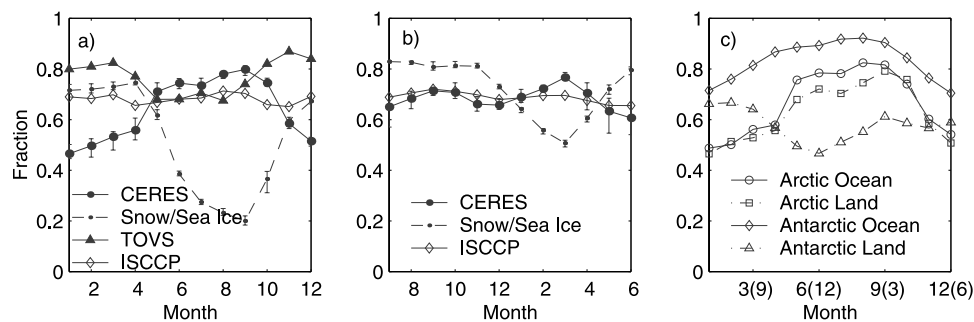


Figure 2. Monthly mean cloud fractions derived from MODIS radiances by the CERES cloud algorithm for (a) the Arctic, (b) the Antarctic, and (c) over ocean surfaces and over land surfaces. Monthly mean snow and sea ice fractions derived from SSM/I are shown by small solid circles. The cloud amounts estimated from TOVS [Schweiger et al., 2002] over the Arctic and International Satellite Cloud Climatology Project (ISCCP) [Schiffer and Rossow, 1983] are shown by closed triangles and open diamond, respectively. The months in parenthesis are for the Antarctic and the error bars are the same as in Figure 1.

beyond the scope of this paper are also in play and should be explored in the future.

3.1. Anomalies

[14] Figure 3 shows time series of the anomalies computed for the Arctic. Because of a large change in daytime snow and sea ice fractions (i.e., only from sunlit regions), the daytime snow and sea ice fractions show a significant (-0.064 ± 0.055 at an 80% confidence level) trend over the 48 months. The trend in the daytime cloud fraction is also statistically significant, but the TOA shortwave irradiance trend is not. Anomalies of the same variables examined for the Antarctic do not show significant trends. The daytime cloud fraction over the Arctic increases at a rate of 0.047 ± 0.041 per decade at an 80% confidence level, which corresponds to a 6.5% relative increase per decade. Auto-correlations are taken into account to assess the uncertainty in the trend by reducing the number of samples using the method of *Wilks* [1995]. This rate is larger than that derived by *Wang and Key* [2005b], who found that the cloud amount derived from AVHRR data increased at rate of 0.016 per decade in summer and 0.033 per decade in spring from 1982 through 1999. However, the latter rates are within the statistical uncertainty of the current results and are from different time period.

[15] The rate of the daytime snow and sea ice and cloud cover change derived from this 48-month period is -0.064 and 0.047 per decade, respectively, while the mean daytime snow/sea ice and cloud fractions are 0.45 and 0.7, respectively. The mean CERES-derived all-sky and clear-sky albedos over the Arctic are 0.47 and 0.38, respectively. If we assume that clouds randomly overlap with snow and sea ice, the clear-sky albedo over land and ocean with no snow/sea ice is 0.15, clouds do not change the albedo over snow and sea ice, the clear-sky and cloudy-sky albedos with and without snow/sea ice on the surface can be estimated. These

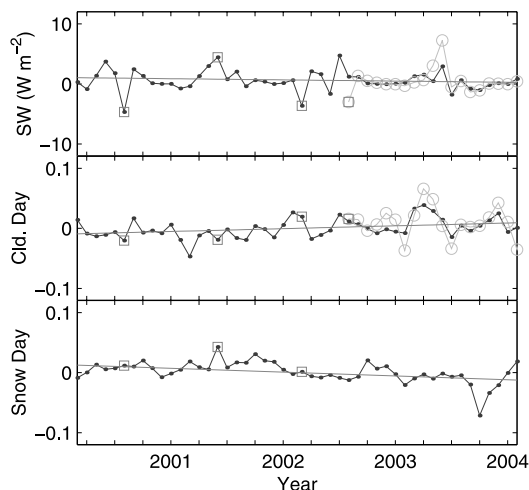


Figure 3. Reflected TOA shortwave irradiance (SW), daytime cloud fraction (Cld. Day), and daytime snow and sea ice fraction (Snow Day), anomalies as a function of month for the Arctic. Terra data are represented by the solid line with dots, and Aqua data by the light solid line with open circles. Open squares indicate months with missing days. The horizontal lines are linear regression fit to Terra data.

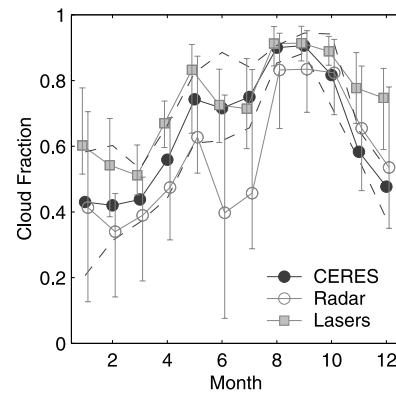


Figure 4. Monthly mean day and nighttime cloud fractions over Barrow, AK from March 2000 through Feb. 2004 (solid lines). The error bars and dashed lines indicate the maximum and minimum values from ground-based active sensors and from the CERES cloud algorithm, respectively, during the 4 years.

estimated albedos suggest that the reflected shortwave irradiance would decrease at a rate of 6.3 Wm^{-2} per decade if clouds are not present, 3.9 Wm^{-2} per decade if the cloud cover stays the same, and 2.2 Wm^{-2} per decade, if cloud cover changes at the observed rate. Therefore, the influence of reduced Arctic sea ice cover on the TOA shortwave irradiance is reduced by the presence of clouds. In addition, the result of the smaller, and less statistically significant, reflected shortwave irradiance trend of $-2.0 \pm 2.0 \text{ Wm}^{-2}$ per decade at an 80% confidence level is, therefore, consistent with the increase in daytime cloud fraction that coincides with the steep decrease in sea ice fraction over the Arctic.

4. Ground-Based Measurements

[16] To increase confidence in the CERES cloud fractions, we compare them with cloud fractions derived from active ground-based instruments. The Atmospheric Radiation Measurement (ARM) program operates a millimeter-wave cloud radar and two laser systems, a micro-pulse lidar and a Vaisala ceilometer, at Barrow, Alaska. The monthly mean CERES cloud amounts derived over the $1^\circ \times 1^\circ$ box that contains Barrow fall between the cloud radar and laser derived cloud fractions [*Clothiaux et al.*, 2000] (Figure 4). The difference of cloud radar and laser-derived cloud occurrence is expected because lasers are the most sensitive sensors easily available for detecting cloud particles, where cloud radars fail to detect smallest cloud particles. The resulting annual mean cloud fractions over Barrow retrieved from the cloud radar and lasers are 0.57 and 0.74, respectively, compared to the CERES annual mean cloud amount of 0.71. See auxiliary material for additional information¹.

5. Summary and Conclusions

[17] Terra data collected from March 2000 through February 2004 suggest that the Arctic daytime cloud cover increased by 0.047 per decade during this period

¹Auxiliary materials are available in the HTML. doi:10.1029/2006GL026685.

while the daytime snow and sea ice fraction decreased at a rate of 0.064 per decade. The trends are significant at an 80% confidence level. The TOA reflected irradiance shows less significant trend during this period, which is consistent with a large cloud cover in summer and with increasing cloud cover with diminishing snow and sea ice cover. While four years of data are usually not enough to detect trends, the CERES data set shows a trend in cloud cover at the 80% confidence level because a relatively large change occurs in this period. The large differences in the CERES and TOVS cloud fractions suggest that optically thin clouds might often be present during the Arctic winter. This result also suggests that the ranges of cloud optical thicknesses retrieved from different instruments needs to be characterized in order to compare cloud fractions from different instruments.

[18] Although based on a limited time series, these results suggest that changes in Arctic sea ice are compensated by changes in cloud cover, perhaps, as a result of enhanced evaporation from the sea surface, therefore, leaving the TOA energy budget unchanged. The implications are that any ice-albedo feedback could be dampened because of increased cloud cover and such responses should be sought in climate simulations. The result of Wang and Key [2005b] suggests that the net shortwave increase at the surface due to the change in sea ice cover is also reduced by increasing the cloud cover. However, much additional work needs to be conducted to confirm these limited results. To reduce the uncertainty in estimating the trend in TOA irradiance and cloud fraction, a longer period of data is necessary. The CERES project will be producing an Edition 3 data set beginning in late 2006. It will be processed with improved angular distribution models and cloud identification algorithms. Thus, further analysis of Arctic cloud cover and radiation trends is left for future research when a better and longer data set, especially for nighttime, becomes available.

[19] **Acknowledgments.** We thank T. Wong of NASA Langley Research Center for providing ERBE values, Y. Chen of SAIC for assisting the data analyses and E. C. Weatherhead and S. G. Warren for helpful comments. ARM data were made available through the U.S. Department of Energy as part of the Atmospheric Radiation Measurement Program. The ERBE and CERES data were obtained from the NASA Langley Atmospheric Science Data Center. The work was supported by a grant from the CERES project (NNL04AA26G), NASA grants (NNG04GL93G, NNG04GL94G, and NNG04GN96G), and Jet Propulsion Laboratory, California Institute of Technology, contract (1259588).

References

- Beesley, J. A., and R. E. Moritz (1999), Toward an explanation of the annual cycle of cloudiness over the Arctic Ocean, *J. Clim.*, *12*, 395–415.
- Clothiaux, E. E., et al. (2000), Objective determination of cloud height and radar reflectivities using a combination of active remote sensors at the ARM CART sites, *J. Appl. Meteorol.*, *39*, 645–665.
- Comiso, J. (2002), A rapidly declining perennial sea ice cover in the Arctic, *Geophys. Res. Lett.*, *29*(20), 1956, doi:10.1029/2002GL015650.
- Curry, A. J., and E. E. Ebert (1992), Annual cycle of radiation fluxes over the Arctic ocean: Sensitivity to cloud optical properties, *J. Clim.*, *5*, 1267–1280.
- Hahn, C. J., S. G. Warren, and J. London (1995), The effect of moonlight on observations of cloud cover at night, and applications to cloud climatology, *J. Clim.*, *8*, 1429–1446.
- Hollinger, J., P. J. L. Peirce, and G. A. Poe (1990), SSM/I instrument evaluation, *IEEE Trans. Geosci. Remote Sens.*, *28*, 781–790.
- Kato, S., and N. G. Loeb (2005), Top-of-atmosphere shortwave broadband observed radiance and estimated irradiance over polar regions from Clouds and the Earth's Radiant Energy System (CERES) instruments on Terra, *J. Geophys. Res.*, *110*, D07202, doi:10.1029/2004JD005308.
- King, M. D., Y. J. Kaufman, W. P. Menzel, and D. Tanre (1992), Remote sensing of cloud, aerosol, and water vapor properties from the Moderate resolution Imaging Spectrometer (MODIS), *IEEE Trans. Geosci. Remote Sens.*, *30*, 2–27.
- King, M. D., et al. (2003), Cloud and aerosol properties, precipitable water, and profiles of temperature and water vapor from MODIS, *IEEE Trans. Geosci. Remote Sens.*, *41*, 442–458.
- Lin, B., P. Minnis, and A. Fan (2003), Cloud liquid water path variations with temperature observed during the Surface Heat Budget of the Arctic Ocean (SHEBA) experiment, *J. Geophys. Res.*, *108*(D14), 4427, doi:10.1029/2002JD002851.
- Loeb, N. G., et al. (2003), Angular distribution models for top-of-atmosphere radiative flux estimation from the Clouds and the Earth's Radiant Energy System instrument of the Tropical Rainfall Measuring Mission satellite: Part I. Methodology, *J. Appl. Meteorol.*, *42*, 240–265.
- Loeb, N. G., S. Kato, K. Loukachine, and N. M. Smith (2005), Angular distribution models for top-of-atmosphere radiative flux estimation from the Clouds and the Earth's Radiant Energy System instrument on the Terra satellite: Part I. Methodology, *J. Atmos. Oceanic Technol.*, *22*, 338–351.
- Loeb, N. G., et al. (2006a), Multi-instrument comparison of top-of-atmosphere reflected solar radiation, *J. Clim.*, in press.
- Loeb, N. G., S. Kato, K. Loukachine, and N. M. Smith (2006b), Angular distribution models for top-of-atmosphere radiative flux estimation from the Clouds and the Earth's Radiant Energy System instrument on the Terra satellite: Part II. Validation, *J. Atmos. Oceanic Technol.*, in press.
- Minnis, P., et al. (2003), CERES cloud property retrievals from imagers on TRMM, Terra, and Aqua, paper presented at 10th International Symposium on Remote Sensing, Conference on Remote Sensing of Clouds and the Atmosphere VII, Soc. of Photo-Opt. Instrum. Eng. (SPIE), Barcelona, Spain.
- Rothrock, D. A., Y. Yu, and G. A. Maykut (1999), Thinning of the Arctic sea-ice cover, *Geophys. Res. Lett.*, *26*, 3469–3472.
- Schiffer, R. A., and W. B. Rossow (1983), The International Satellite Cloud Climatology Project (ISCCP): The first project of the World Climate Research Programme, *Bull. Am. Meteorol. Soc.*, *64*, 779–784.
- Schweiger, A. J., R. W. Lindsay, J. A. Francis, J. Key, J. Intrieri, and M. Shupe (2002), Validation of TOVS Path-P data during SHEBA, *J. Geophys. Res.*, *107*(C10), 8041, doi:10.1029/2000JC000453.
- Stroeve, J. C., et al. (2005), Tracking the Arctic's shrinking ice cover: Another extreme September minimum in 2004, *Geophys. Res. Lett.*, *32*, L04501, doi:10.1029/2004GL021810.
- Wang, X., and J. Key (2005a), Arctic surface, cloud and radiation properties based on the AVHRR polar pathfinder dataset: Part I. Spatial and temporal characteristics, *J. Clim.*, *15*, 2558–2574.
- Wang, X., and J. Key (2005b), Arctic surface, cloud and radiation properties based on the AVHRR polar pathfinder dataset: Part II. Recent trend, *J. Clim.*, *15*, 2575–2593.
- Wielicki, B. A., et al. (1996), Clouds and the Earth's radiant energy system (CERES): An Earth observing system experiment, *Bull. Am. Meteorol. Soc.*, *77*, 853–868.
- Wilks, D. S. (1995), *Statistical Methods in the Atmospheric Sciences*, p. 127, Elsevier, New York.

T. P. Charlock, S. Kato, N. G. Loeb, and P. Minnis, Climate Science Branch, NASA Langley Research Center, Mail Stop 420, Hampton, VA 23681-2199, USA. (s.kato@larc.nasa.gov)

E. E. Clothiaux, Department of Meteorology, Pennsylvania State University, 603 Walker Bldg, University Park, PA 16802, USA.

J. A. Francis, Institute of Marine and Coastal Sciences, Rutgers University, 71 Dudley Rd., New Brunswick, NJ 08901, USA.

D. A. Rutan and S. Sun-Mack, Mail Stop 927, NASA Langley Research Center, Hampton, VA 23681-2199, USA.